Measurement of forces on multi-point forming tools using Fibre Bragg Grating sensors

Elghawail, Ali; Pham, Duc; Huang, Jun; Su, Shizhong; Kerin, Mairi; Ji, Chunqian; Abosaf, Mohamed; Essa, Khamis

DOI:
10.1177/0954405419875334

Document Version
Peer reviewed version

Citation for published version (Harvard):
Elghawail, A, Pham, D, Huang, J, Su, S, Kerin, M, Ji, C, Abosaf, M & Essa, K 2019, 'Measurement of forces on multi-point forming tools using Fibre Bragg Grating sensors', *Proceedings of the Institution of Mechanical Engineers Part B Journal of Engineering Manufacture*. https://doi.org/10.1177/0954405419875334

Measurement of Forces on Multi-Point Forming Tools Using Fibre Bragg Grating Sensors

Ali Mohamed Elghawail, Duc Truong Pham, Jun Huang*, Shizhong Su, Mairi Kerin, Chunqian Ji, Mohamed Abosaf and Khamis Essa

Department of Mechanical Engineering, School of Engineering, University of Birmingham, Birmingham B15 2TT, UK

Corresponding author: j.huang.1@bham.ac.uk (J. Huang)

Abstract:

Multi-point forming (MPF) uses forces applied to a tool, comprising of multiple pins set at different heights, to form sheet metal for panelling in white goods, automotive bodywork and aircraft frames etc. The use of multiple pins allows for rapid change over and flexibility in the tool making it suitable for small-batch and prototype component manufacture. To explore the relationship between "springback" of the sheet metal on release from the tool, and the applied pin force, it is first necessary to understand and measure the forming forces.

This paper presents a novel method of measuring forming forces on individual pins in a MPF tool using Fibre Bragg Grating (FBG) sensors, monitoring the elastic strain on the selected pins during the forming process. The operating principles behind forming force measurements using FBGs are introduced and a relationship is developed between springback in the formed part after the final unloading, and the forming force as measured on selected individual pins under different compression ratios (30%, 40%, 50% and 60%) of the elastic cushion between the tips of the pins and the workpiece. Experiments were performed to validate the proposed measuring method and results indicate that forming forces detected by the proposed method correlated well with the results obtained by numerical simulation. This suggests the proposed method has good potential for real-time measurement and monitoring of forming force distribution in MPF tools during the forming process.

Keywords: Multi-point Forming, Forming Force, Force Measurement, Fibre Bragg Grating Sensor

1. Introduction

Multi-point forming (MPF) is a kind of flexible metal sheet forming technique with reconfigurable dies for 3D surfaces with low manufacturing costs compared with solid dies in industrial applications such as aerospace, architecture and automobiles [1-3]. Figure 1 is a schematic diagram of a MPF tool [4]. This shows the pin matrices (MPF-Punch and MPF-Die), the elastic cushions and the workpiece (metal sheet) sandwiched between the elastic cushions. MPF technology was utilised for rapid fabrication of 3D sheet metal parts using two reconfigurable element groups with height-adjustable pins (continuous upper and lower solid dies) [5, 6]. A multi-point matched-die forming technique and its typical applications were reported [7]. A flexible hybrid sheet forming process combining multi-point forming (MPF) and incremental sheet forming (ISF) was employed for the control of the thickness of metal parts [8].

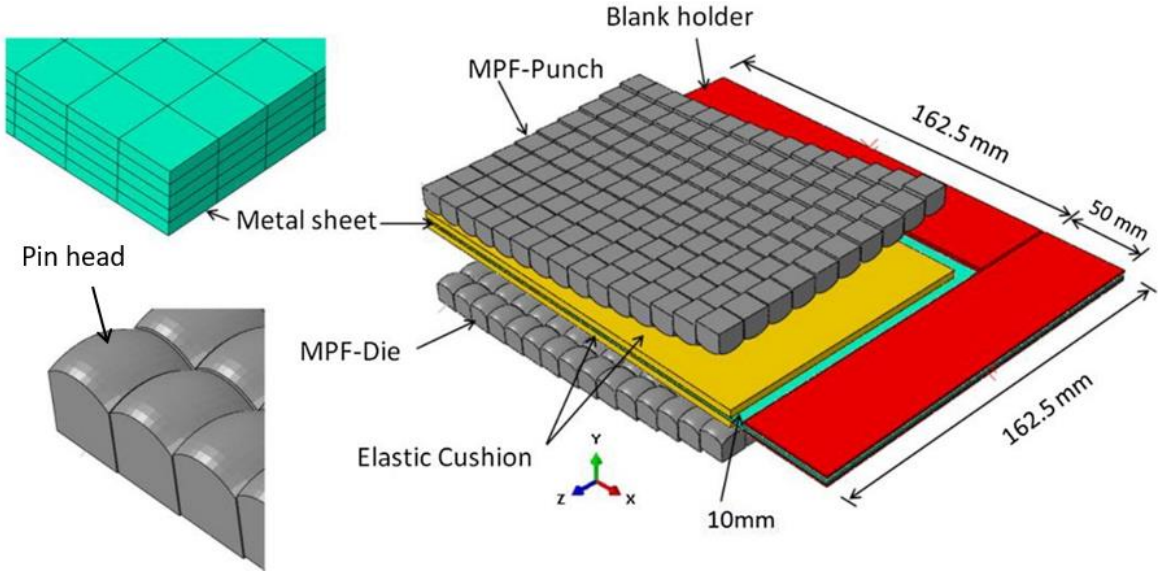

Figure 1. Schematic diagram of a MPF tool [4]

The MPF process parameters including the elastic cushion thickness, coefficient of friction, pin size and radius of curvature were investigated and optimised [9]. Springback is a common defect in sheet metal processes and needs to be minimised or compensated for, depending on part usage [10]. The forming parameters influencing springback in a MPF process were investigated by experiments and finite element simulations [11]. Numerical investigations of a MPF process were carried out, which covered wrinkling, dimpling and springback [12]. With individually controlled force-displacement, a new MPF process was presented to reduce springback [13]. The forming parameters such as the hardness and thickness of the elastic

cushion, blank holder force, coefficient of friction and radius of curvature were investigated and optimised to improve the quality of parts using MPF [14].

Forming force measurements are essential for the investigations of MPF processes to avoid defects and improve forming precision. To detect forming forces on individual pins in MPF tools within a narrow working area requires sensors with high specifications. FBG sensors have a series of unique advantages over conventional electrical and piezoelectric sensors, including high precision, small size (125 μm diameter with cladding), lightweight, immunity to electromagnetic interference, distributed measurement and ease of installation [15, 16]. FBG sensing technology has found many uses in manufacturing and industry [17, 18].

FBGs can deliver sensitive and distributed strain and force measurements for different materials and structures [19, 20]. FBG sensors embedded into polymer composite materials were adopted for strain measurements [21]. An experimental method using FBGs for strain measurements of wooden structures was presented and validated [22]. FBG sensors were embedded in a 3D printed sensor structure for mechanical strain measurements [23]. FBG sensors were employed for quasi-distributed dynamic strain measurement and strain modal analysis of hydraulic system pipelines [24, 25]. Embedded FBGs were used to monitor strain in aluminium alloys during production [26]. Multipoint strain measurement in an NbTi superconducting sample coil was carried out using FBG sensors at low temperature and in a high background magnetic field [27]. FBG sensors were employed to measure strain and temperature induced during micro-turning operations [28].

Force sensitive forceps with an FBG sensor on the grasper were proposed for a surgical robot in a surgery environment [29]. A bolt force status monitoring method using FBG sensors was proposed for remote real-time monitoring of roadway anchorage engineering [30]. A FBG based transverse force sensor was presented and experimentally demonstrated [31]. A method of measuring bending force and temperature was proposed [32]. A FBG six degree-of-freedom force-moment sensor was developed for a surgical robot [33] and FBG sensors were used to monitor inner forces of a reinforced concrete frame-shear wall structure [34].

The work reviewed above highlights the extensive use of FBG sensors in strain and force measurements. However, there has been no reported research into using FBG sensors in MPF tooling. The aim of this paper is to present a novel method suitable for detecting and analysing real-time forming forces on individual pins in MPF tools. By measuring the forces on strategically located pins, the force distribution on MPF tools could be obtained to

optimise MPF process parameters for springback reduction. The proposed measurement method uses FBG sensors to monitor the elastic strain on pins of MPF tools. The paper is organised as follows: Section 2 introduces the operating principles of forming force measurement using FBG sensors. An analysis of forming forces on MPF tools using numerical simulations is described in Section 3. Section 4 reports on experiments to measure forming forces using FBG sensors. Section 5 concludes the paper and provides suggestions for further work.

2. Operating principles of forming force measurement

The operating principles of forming force measurement are investigated in this section. The sensing principle of FBG is introduced and the method of forming force measurement using FBG is outlined.

2.1 Sensing principle of FBG

FBG is a kind of distributed Bragg reflector (Bragg grating) built into an optical fibre. When light from a broadband source is incident on one side of the reflector, the inscribed Bragg gratings act as a mirror reflecting certain wavelengths while passing the rest. FBG sensors could be added to the surface of a pin to obtain real-time information on the strain on it.

The Bragg wavelength reflected by the grating (λ_B), depends mainly on the fibre grating periodicity (Λ) and the effective refractive index (n_{eff}). It is calculated using the following equation [35]:

$$\lambda_B = 2n_{eff}\Lambda \tag{1}$$

Both strain and temperature affect the Bragg wavelength, as both change the grating periodicity, the latter due to the thermal expansion/contraction through the thermo-optic and thermal expansion coefficients.

Thus, any change in the refractive index of the fibre grating and/or fibre grating periodicity will cause a change in the wavelength of the reflected light from λ_{B0} to λ_B where the subscript "$_0$" refers to the original condition. Thus, the reflected wavelength can be regarded as a function of strain (ε) and temperature (T), and its change can be written as follows [35]:

$$\Delta\lambda_B = \lambda_B(\varepsilon, T) - \lambda_{B0}(\varepsilon_0, T_0) \tag{2}$$

Expanding Equation (2) as a Taylor series and taking a first-order approximation, then for a fibre with a coefficient of thermal expansion (α_t), thermo-optic coefficient (α_n) and photo-elasticity coefficient (p_e) then wavelength shift can be expressed as [36]:

$$\Delta\lambda_B = \lambda_B[(1 - p_e)\Delta\varepsilon + (\alpha_t + \alpha_n)\Delta T] \quad (3)$$

where $\Delta\varepsilon$ is the change in strain of the optical fibre, and ΔT is the temperature change. Generally, the temperature of the environment remains more or less constant and temperature effects could be neglected during a quick measurement. Thus, any shift in the Bragg wavelength ($\Delta\lambda_B$) will be caused by applied strain (extending or compressing the grating) and the photo-elastic effect as given in Equation (3).

2.2 Forming force measurement

The basic operation of forming force measurement as carried out on four individual pins is shown on a quarter of the 3D FE model in Figure 2. A "smart" sensorised individual forming force tool is constructed by installing a FBG sensor axially along the pin. Each FBG attached to each pin reflects with a different wavelength allowing real-time information on total change in strain to be obtained for that chosen pin.

The schematic diagram in Figure 2 shows the system used to measure forming forces of MPF tools (punch and die) including FBG sensors installed on the pins' longitudinal surfaces, a data acquisition system and analysis devices. A multi-channel FBG interrogator is employed to acquire the elastic strain change signals from the FBGs. The collected data for elastic strain is analysed and evaluated by a computer.

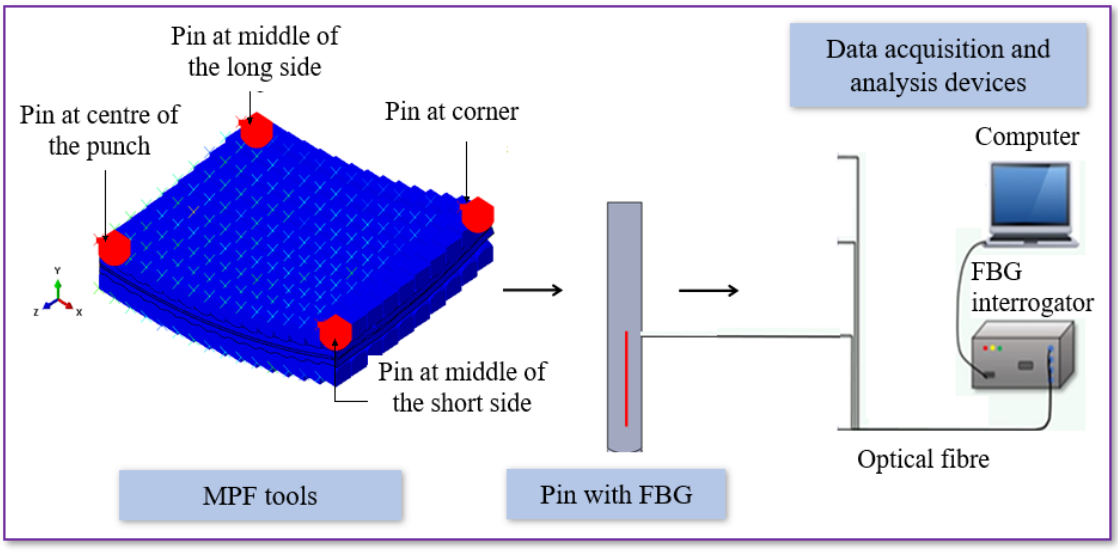

Figure 2. Measurement system for forming force on individual pins (quarter MPF tool)

As shown in Figure 2, FBG sensors are attached to monitor the elastic strain of the four pins during sheet forming. The strain is proportional to the magnitude of the forming force. Assuming that temperature effects are negligible as the surrounding environment temperature is stable ($\Delta T = 0$), Equation (3) can be re-written as:

$$\frac{\Delta\lambda_B}{\lambda_{B0}} = k\Delta\varepsilon \tag{4}$$

where k = (1- p_e) and p_e = 0.22 (photo-elastic coefficient), then k = 0.78×10^{-6} $\mu\varepsilon^{-1}$. Substituting these values into Equation 4, we obtain:

$$\frac{\Delta\lambda_B}{\Delta\varepsilon} = 0.78 \times 10^6 \mu\varepsilon^{-1} \times \lambda_B \tag{5}$$

From Equation (5), it can be calculated that when the FBG is strained by 1 $\mu\varepsilon$ the reflected Bragg wavelength increases by 1.21 *pm* for a FBG with a centre wavelength of 1550 nm [37]. The initial wavelength of the sensor is known, and k is constant. The elastic strain (ε) on pins under the forming force could be calculated using Equation (6):

$$\varepsilon = \frac{\sigma}{E} = \frac{F}{AE} \tag{6}$$

where F is the force on the pin, A is the cross-section area of the pin and E is Young's modulus of the pin's material. According to Equation (4) and Equation (6), the forming force on pins could be calculated using Equation (7):

$$F = \frac{\Delta\lambda_B}{k\Delta\lambda_{B0}} AE \tag{7}$$

As shown in Figure 3, the forming force does not act vertically on every pin but depends on the pin's position and shape. The forming force is vertical on the pins at the centre of the MPF tool, but it will gradually incline away from the vertical depending on the radius of forming curvature until, at the edges of the MPF tool, it reaches the maximum degree of inclination. Equation (7) could be applied to calculate the local force on the pin.

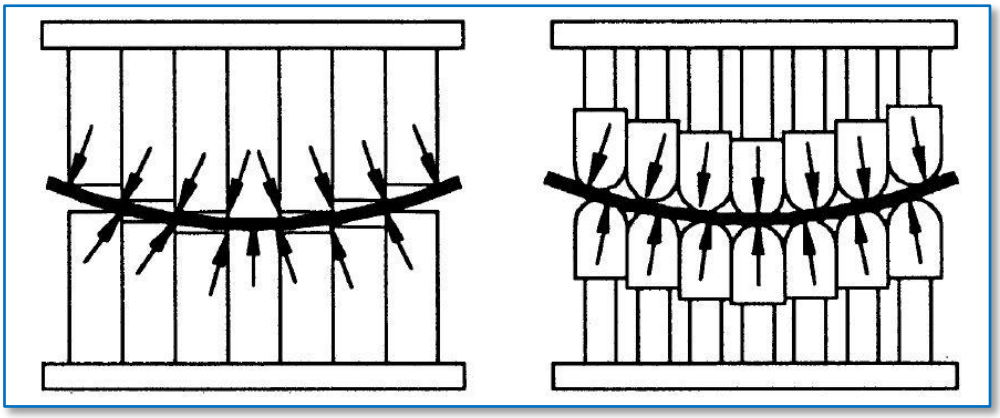

Figure 3. Different pin shapes with different force distributions [38]

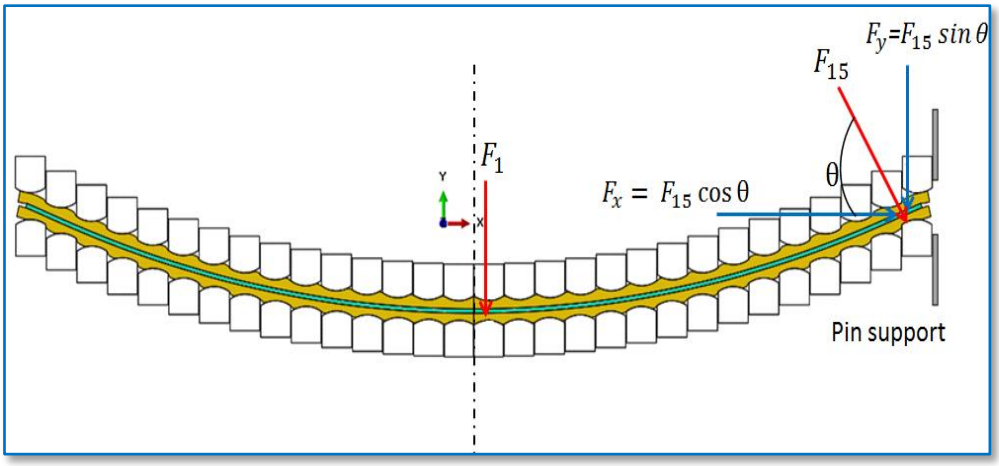

Figure 4. Force distributions on different pins (R = 800 mm)

For small values of radius of curvature (R ≤ 400 mm), the height difference between the pins is relatively large. In this case, the forming force distribution will be different from that for a large radius of curvature (R = 800 mm) because the difference between the pin heights is smaller, as shown in Figure 4. Consequently, at the end of the loading step, the values of the force on the same pin at the same position in the two cases will be different, as shown in Figures 5 (a) and (b). The simulation results are for a 40% compression ratio of the same pin at the centre of punches with 800 mm and 400 mm radii of forming curvature.

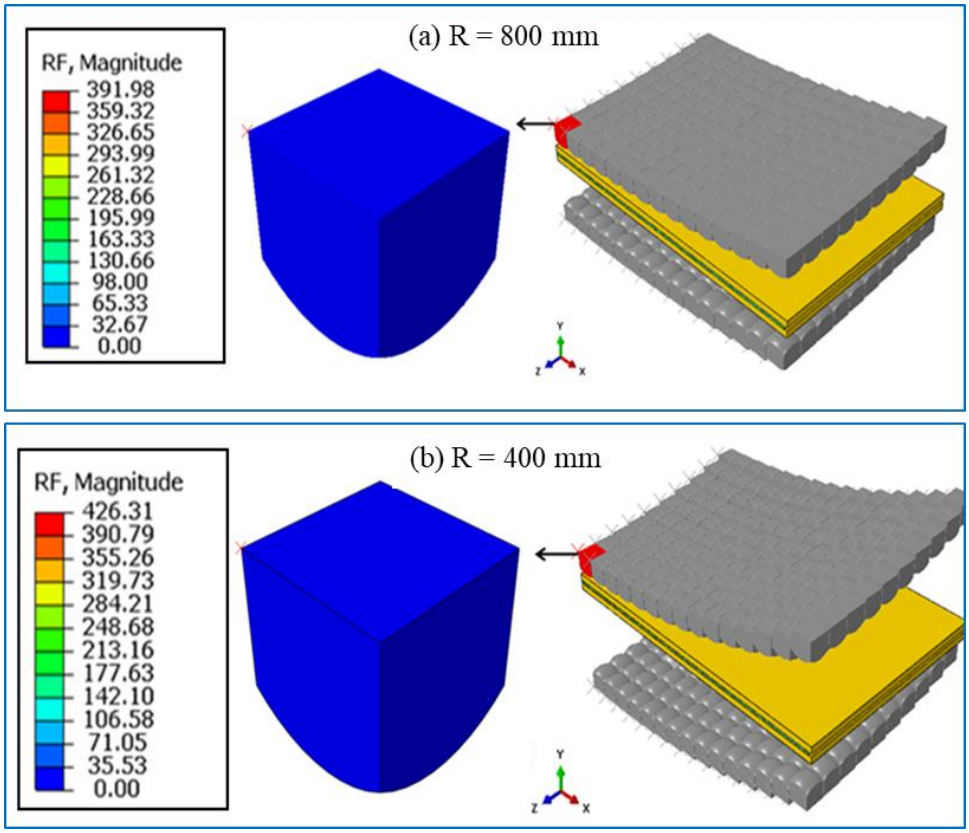

Figure 5. Forming force on a pin at the centre of the punch for different forming radii

Figure 6 shows the simulated force results on the selected pins at different positions in the two cases. As the radius of forming curvature increases, the force distributions become uniform due to smaller differences between pin heights.

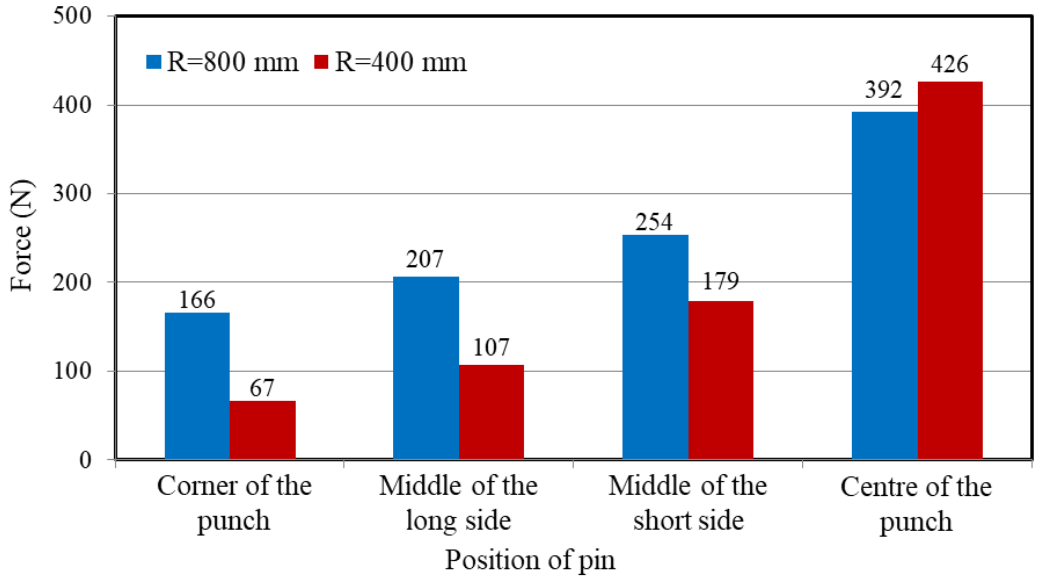

Figure 6. Forces on individual pins for different radii of forming curvature

3. Numerical simulation

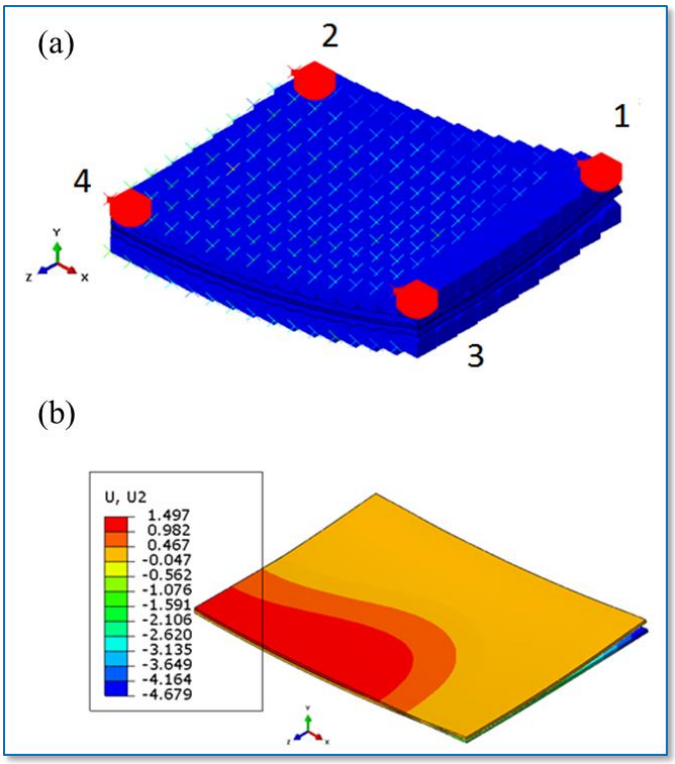

Figure 7. (a) Positions of selected pins and (b) simulated springback value after unloading for 40% compression ratio of elastic cushion

To verify the proposed method of forming force measurement on individual pins of MPF tools, numerical simulation (finite element analysis, FEA) was carried out using ABAQUS software. Figure 7(a) shows the positions of selected pins in an MPF tool. Pin 1 is at the corner of the MPF tool where maximum springback occurs. Pins 2 and 4 are respectively situated in the middle of the long and short sides of the MPF tool with less springback. Pin 4 is located at the centre of the tool with minimum springback. The simulated results for springback at the end of the unloading step in a MPF process with 800 mm as radius of forming curvature are shown in Figure 7(b).

Figure 8 shows the elastic cushion subjected to different compression ratios of its original thickness (3 mm). For example, 40% compression ratio of a 3mm-thick elastic cushion means 0.4 × 3 mm = 1.2 mm and when the punch reaches the end of the forming distance, it will move downward 1.2 mm. A general contact algorithm was used to model the interaction between the elastic cushion and the tips of the MPF tool[1]. Coulomb friction of 0.1 was used to model the contact between the elastic cushion and pins as well as the elsatic cushion and sheet metal. The simulated forming forces on individual pins at different compression ratios of the elastic cushion are shown in Figure 9. It is clear that the force on the selected pins rises

as the punch moves down and increases the compression ratio of the elastic cushion (30%, 40%, 50% and 60%) without causing dimpling of the formed sheet.

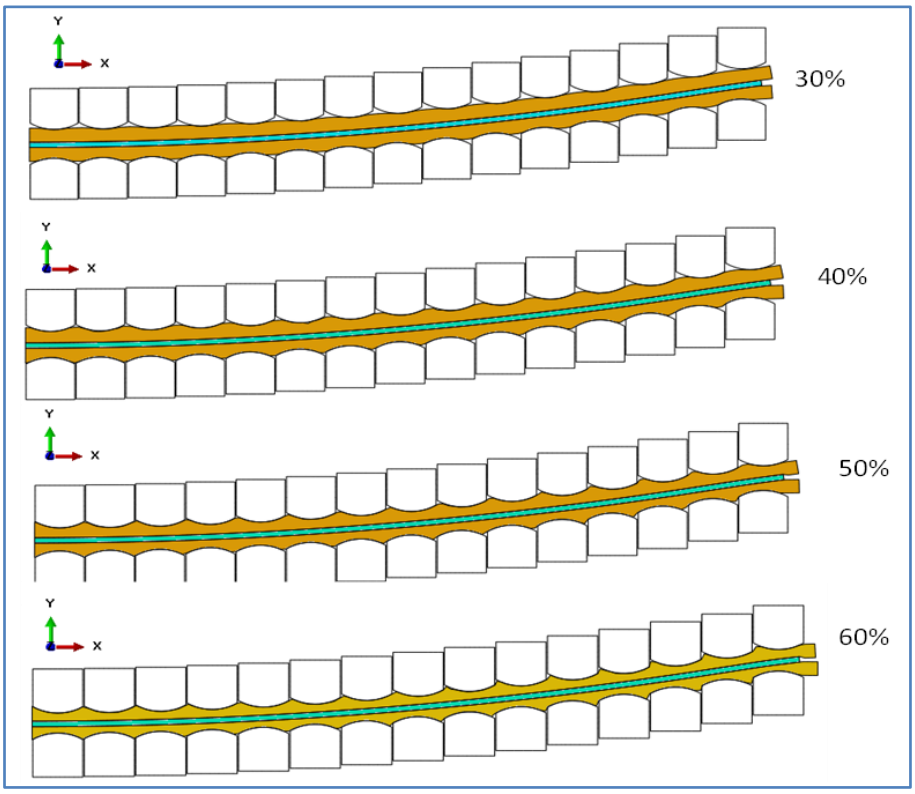

Figure 8. Simulation results for different elastic cushion compression ratios

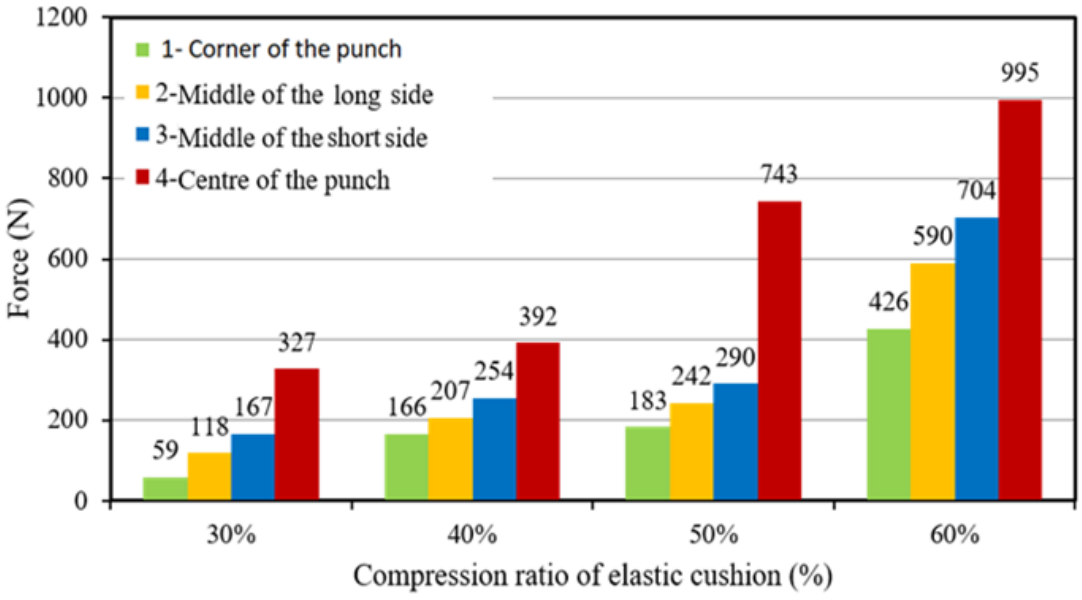

Figure 9. Forming forces on individual pins

Figure 10 shows the relationship between springback of the final formed part (R = 800 mm) at the end of the loading step for different compression ratios of the elastic layer and the

values of the forming force on the selected pins. For example, at a 30% compression of the elastic layer, the forming force on the pin at centre of MPF punch was over 300 N and springback more than 6.5 mm, while at 60% compression the force was nearly 1000 N and the springback approximately 5.0 mm.

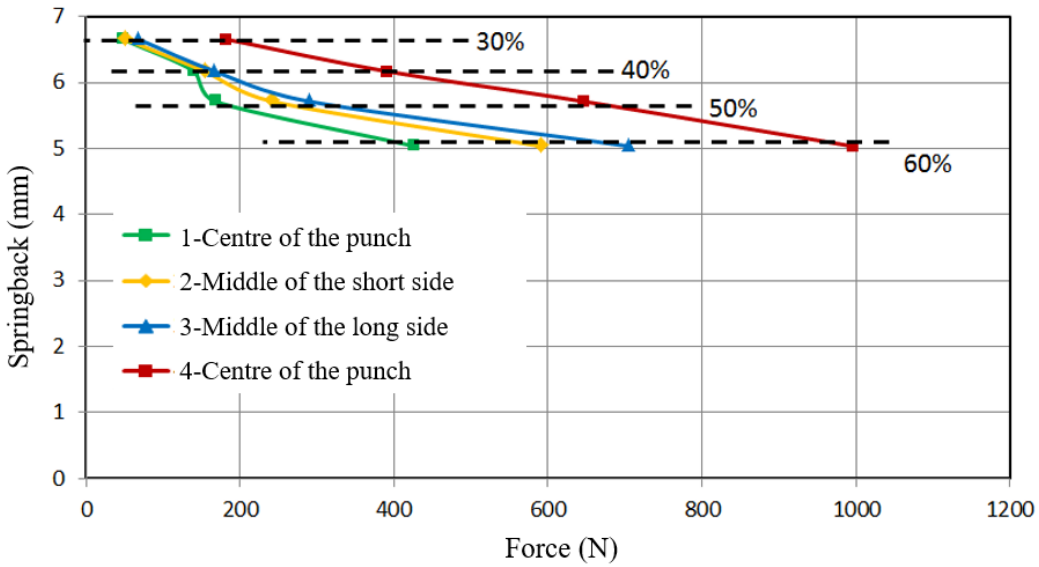

Figure 10. Springback vs force on different pins for different compression ratios

There was a sharp increase in the force on the pin, as the space between the pin tips became filled with elastic material due to the increased compression ratio, see Figure 8. This caused more resistance to movement of the MPF punch. As a result the local force increased and springback decreased.

4. Experiment setup and results

4.1 Static calibration

To obtain the sensitivity of the FBG sensors on the pins, static calibration experiments were carried out using the setup shown in Figure 11. A universal test machine from Instron was employed to apply compressive forces on a pin fitted with a FBG sensor. The pin was secured on the workbench of the machine by a clamping vice. The forces applied on the pin changed from 0 to 10 kN in increments of 2 kN. A 4-channel FBG interrogator (SmartScan from Smart Fibres Ltd, [39]) was used to record the wavelength changes of FBG sensors with a resolution of 1 pm and a maximum acquisition rate of 2.5 kHz per channel. The Young's modulus of the pin material is approximately 200 GPa and the cross section area of the pin is 10 mm × 10 mm [40].

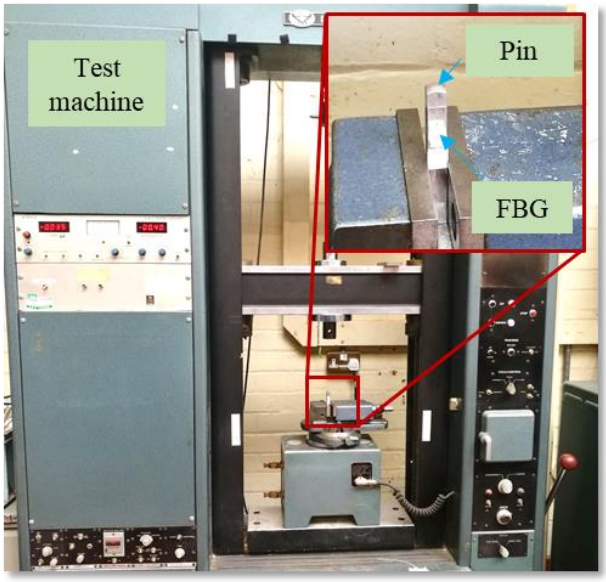

Figure 11. Experimental setup of static calibration

Figure 12 illustrates the wavelength shift of the FBG versus the compressive forces on the pin. The experiments ware repeated six times with the force being increased and then decreased to demonstrate the repeatability of the FBG sensor, as shown in Figure 12 (a). Figure 12 (b) shows the average wavelength shift versus force. The relationship between wavelength shifts and force could is given by Equation (8) which was obtained by linear fitting.

$$\Delta\lambda_B = -69.7F - 2.55 \tag{8}$$

The force sensitivity of the FBG sensor is -69.7 pm/kN and the fitting linear correlation coefficient is 99.97%. The force sensitivity of the FBG sensor is -60.5 pm/kN calculated from Equation (7).

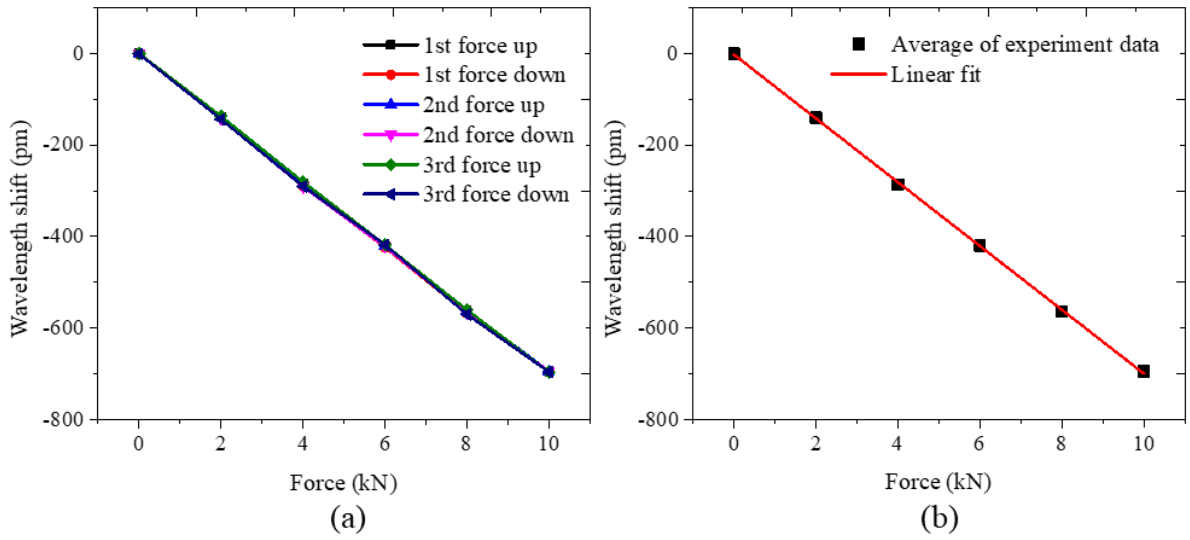

Figure 12. Static calibration results

4.2 Forming force measurement

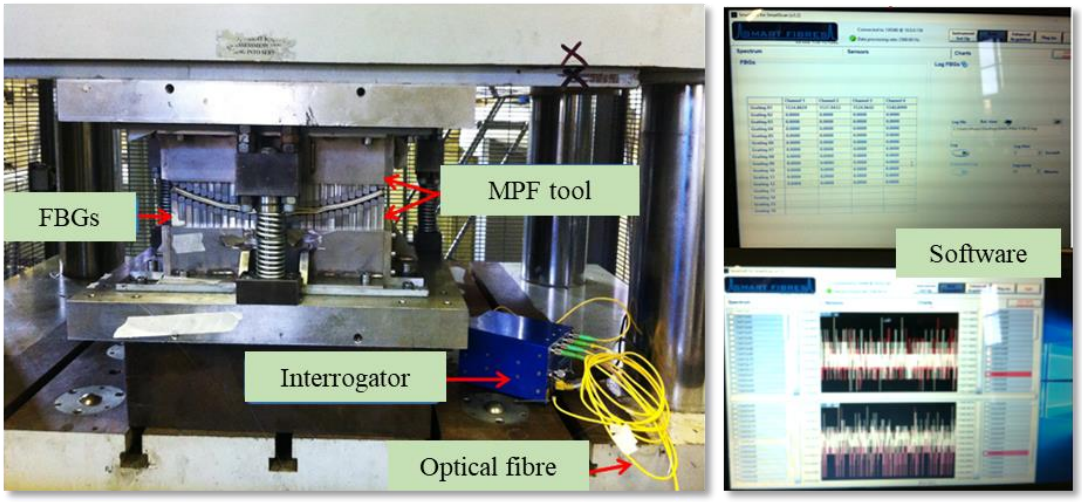

Figure 13. Experimental setup of forming force measurement

Experiments were carried out to test the proposed "smart" way of forming force measurement on pins of MPF tools. Figure 13 shows the experimental setup including an MPF tool installed on a 200-tonne Mackey Bowley press, FBG sensors, a FBG interrogator and optical fibres.

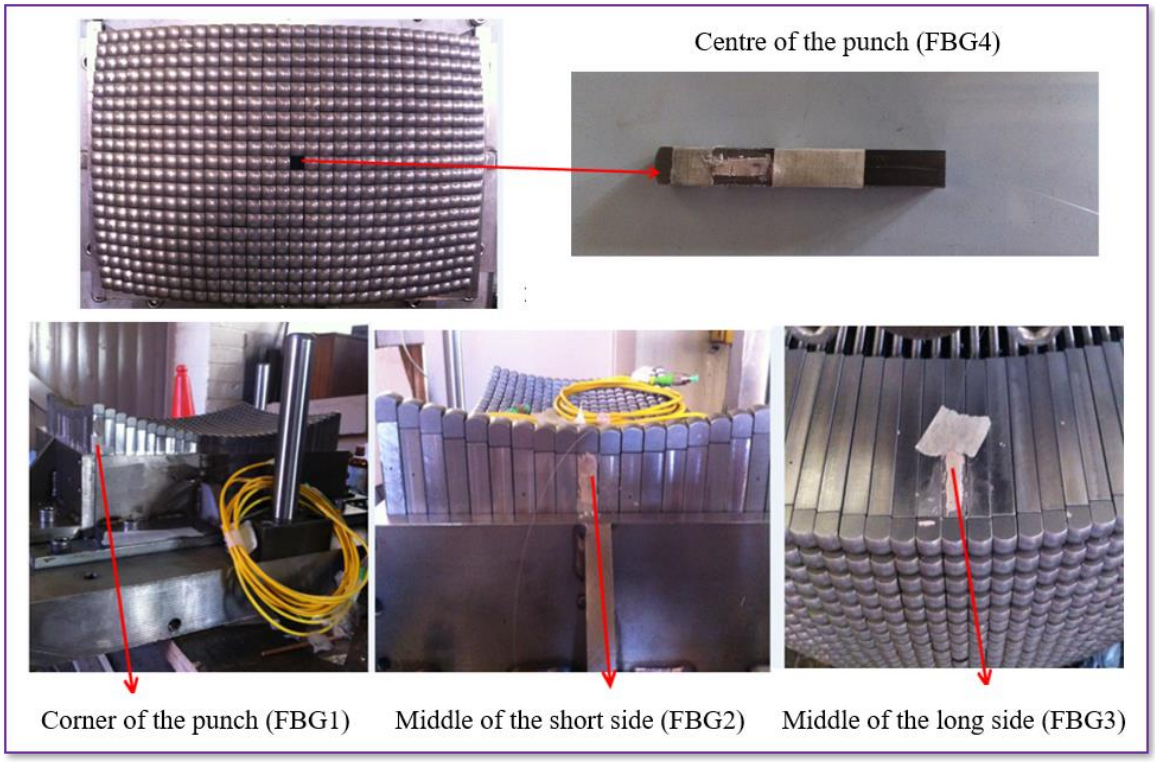

Figure 14. Locations of selected pins on MPF tool

Figure 14 shows the locations of the selected pins on the MPF tool. Each candidate pin used to measure the forming force was fitted with an FBG sensor. Before the bonding of the FBG

sensors to the pins, it was important to prepare the pin's surface to avoid introducing measurement errors such as strain transfer between compressed pin and FBG sensor. The press was adapted for loading the MPF tool to form sheets of 1.2 mm thick in aluminium alloy O-5251, with a radius of forming curvature of 800 mm. For this operation, springback on the final formed part was large.

The wavelength changes and forming time histories were recorded for all four pins during the forming process. As an example, data collected for FBG4 on the pin at the centre of the punch is shown in Figure 15.

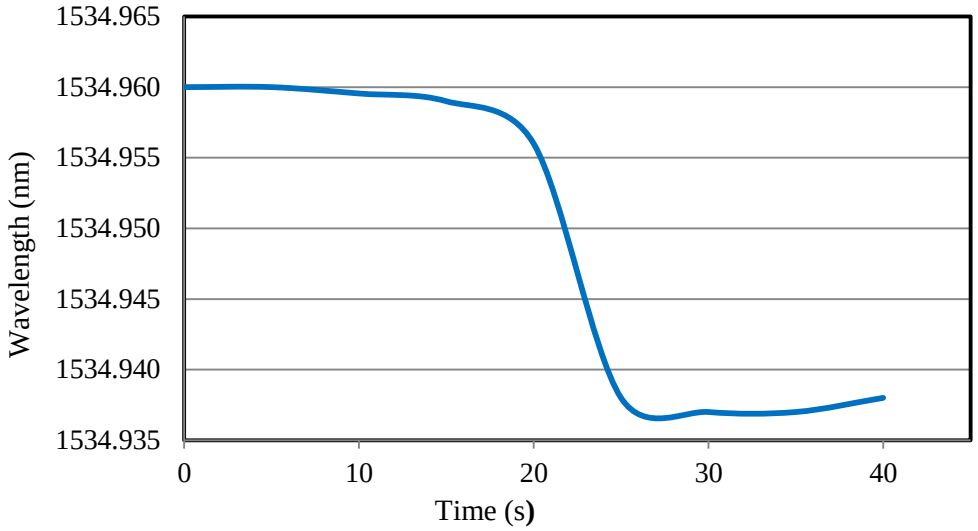

Figure 15. Wavelength shift of FBG4 versus time on the pin at the centre of MPF punch

For the first five seconds, the movement of the punch takes up the slack in the system and no change in wavelength is observed. As the punch continues to move down it starts to compress the elastic cushion, and from about 5 seconds to about 17 seconds, the wavelength of the FBG changes as the cushion is increasingly compressed (see Figure 7). At about 17s the rate of decrease in the FBG wavelength rises significantly as the forming process starts. The sharp fall in wavelength continues until at about 25s the wavelength plateaus due to the compression strain in the pin at the end of the forming process. At about 40s, the load is released.

Table 1. Wavelength changes of FBG sensors under forming force

Process steps	Time (s)	Wavelength (nm)							
		FBG1	$\Delta\lambda_{B1}$	FBG2	$\Delta\lambda_{B2}$	FBG3	$\Delta\lambda_{B3}$	FBG4	$\Delta\lambda_{B4}$
Before loading	0	1534.882	0	1540.897	0	1537.942	0	1534.960	0
Forming process	5	1534.882	0.000	1540.896	-0.001	1537.941	-0.001	1534.960	0.000
	10	1534.882	0.000	1540.895	-0.002	1537.940	-0.002	1534.959	-0.001
	15	1534.881	-0.001	1540.895	-0.002	1537.938	-0.004	1534.957	-0.003
	20	1534.879	-0.003	1540.893	-0.004	1537.936	-0.006	1534.956	-0.004
	25	1534.873	-0.009	1540.885	-0.012	1537.930	-0.012	1534.938	-0.022
	30	1534.872	-0.010	1540.885	-0.012	1537.926	-0.016	1534.937	-0.023
	35	1534.873	-0.009	1540.889	-0.011	1537.927	-0.015	1534.937	-0.023
Loading release	40	1534.874	-0.008	1540.891	-0.009	1537.931	-0.011	1534.941	-0.019
Max. $\Delta\lambda_B$			-0.010		-0.012		-0.016		-0.023

As previously mentioned, the sensitivity of the FBG sensor is typically 1.2 pm/με Table 1 lists the extracted wavelengths of FBGs at several time points in the forming process. According to Equation (7), the maximum forces on each pin can be calculated using the data in Table 1, as shown in Figure 16. In order to evaluate the measurement accuracy of the forming forces on the pins, a comparison between the simulated and measured forces for each pin is shown in Figure 17.

Also the numerical error has been calculated as below:-

$$Numerical\ error = \frac{Experimental\ result - Simulation\ result}{Experimental\ \ result} \times 100\% \quad (9)$$

Figure 18 shows that the numerical errors are small, which indicates that the proposed measurement method was able to measure forming forces accurately.

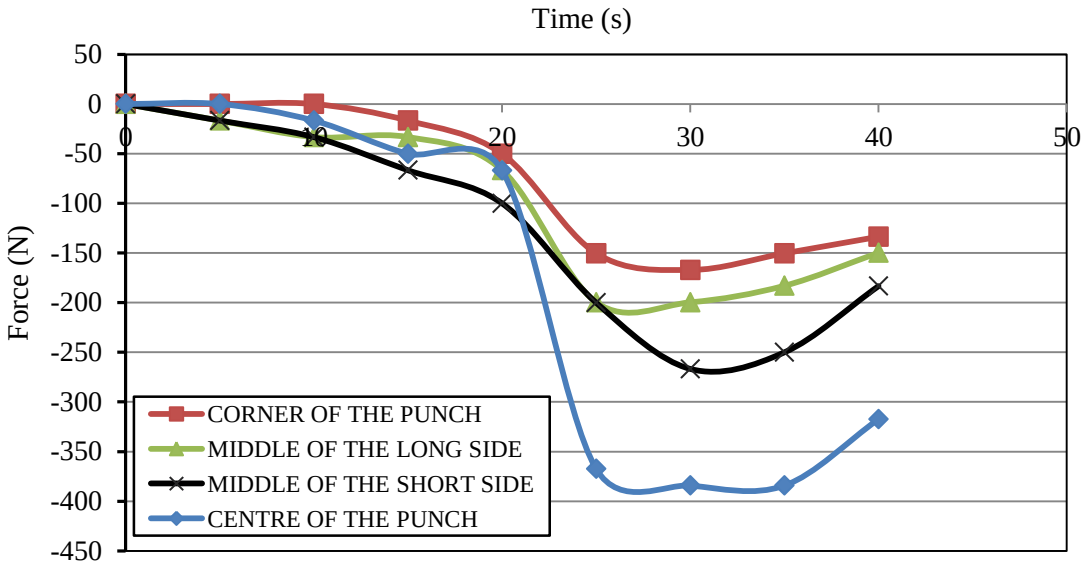

Figure 16. Force – time curve for different pin locations

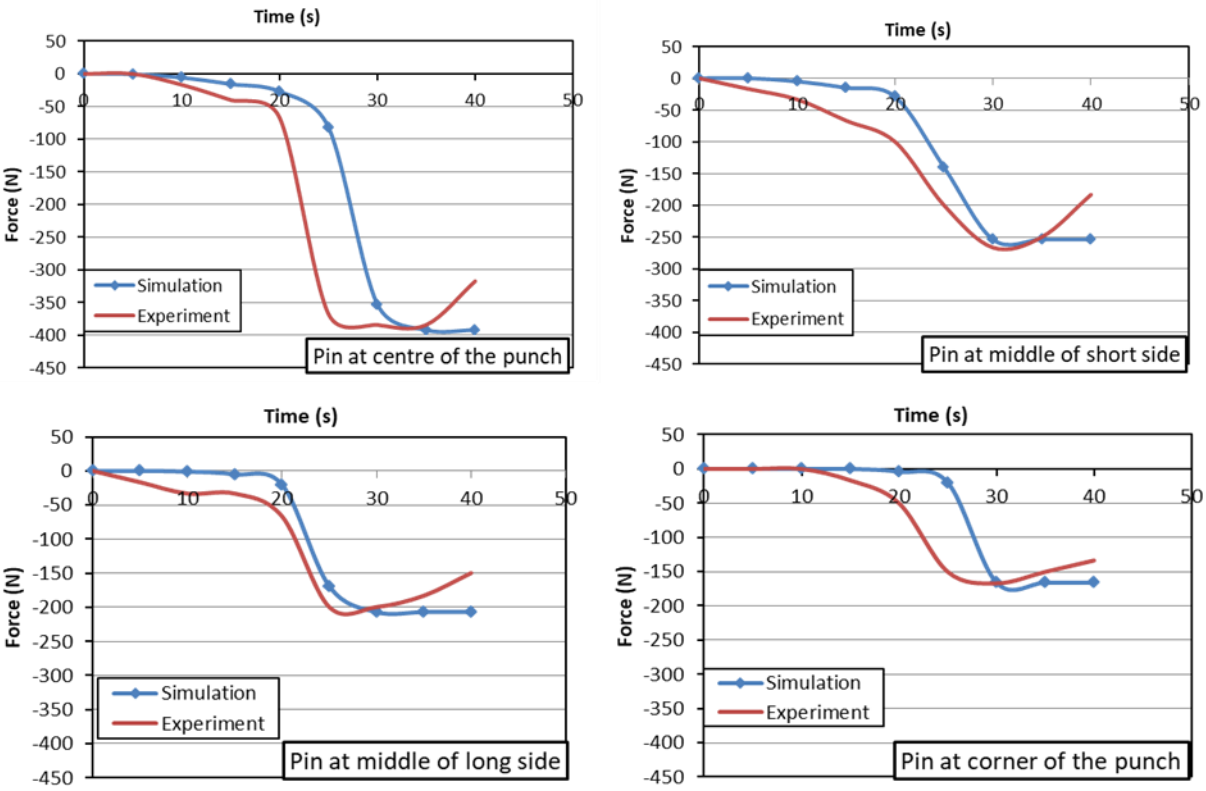

Figure 17. Comparison between simulation and experimental force trends for selected pins

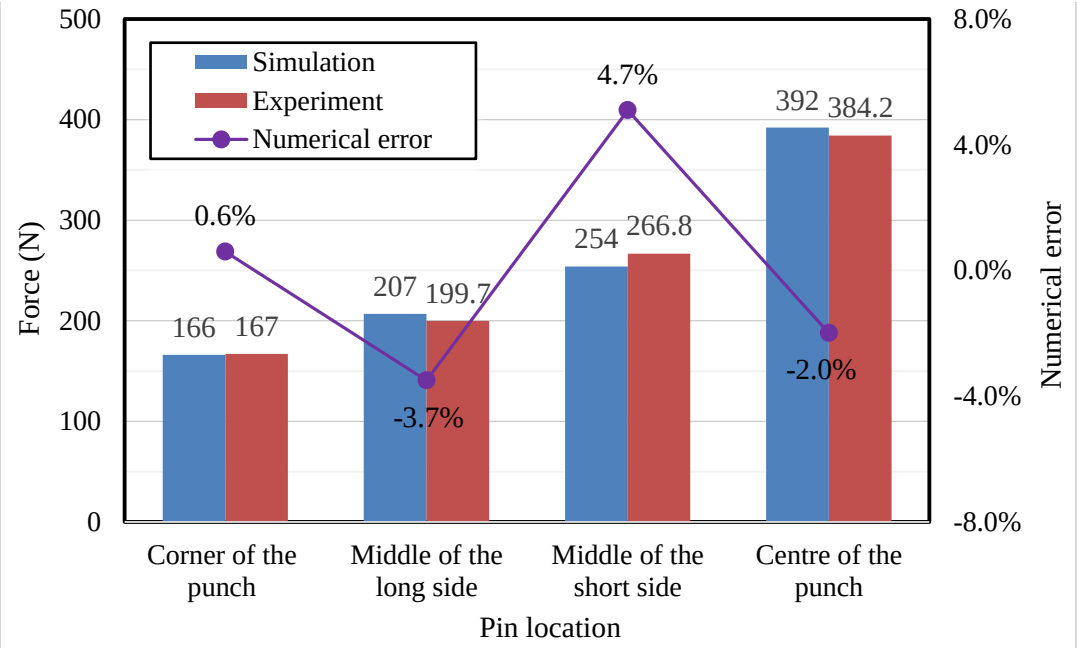

Figure 18. Validation of simulated forming force for radius of forming curvature 800 mm

5. Conclusions

In this paper, a method of forming force measurement in MPF tools using FBG sensors has been presented and validated for the first time. FBG sensors were employed to measure the forming force on individual pins by monitoring the elastic strain in the forming process. The operation principle of the proposed measurement method was introduced. The paper investigated the effect on springback of forming radius curvature and the forming force on selected pins. Experiments were carried out to validate the measuring method. Experimental results show that forming forces measured by the proposed method are in good agreement with those obtained by numerical simulations. The proposed method offers a good solution to measure or monitor forming force distribution on individual pins of MPF tools. Future work will focus on temperature compensation for the proposed forming force measurement method to increase its accuracy.

Acknowledgments

This research is supported by the Engineering and Physical Sciences Research Council (EPSRC) and Innovate UK (Grant EP/L505225/1).

Declaration of conflicting interests

The author(s) declared no potential conflicts of interest with respect to the research, authorship, and/or publication of this article.

References:

1. Elghawail A, Essa K, Abosaf M, et al. Low-cost metal-forming process using an elastic punch and a reconfigurable multi-pin die. *International Journal of Material Forming* 2018. DOI: 10.1007/s12289-018-1423-6.

2. Li M-Z, Cai Z-Y, Sui Z, et al. Multi-point forming technology for sheet metal. *Journal of Materials Processing Technology* 2002; 129: 333-338.

3. Hu Z, Wang C, Chen X, et al. A novel forming method for three-dimensional thin sheet metal. *Proceedings of the Institution of Mechanical Engineers, Part B: Journal of Engineering Manufacture* 2016; 230: 1751-1755.

4. Elghawail A, Essa K, Abosaf M, et al. Prediction of springback in multi-point forming. *Cogent Engineering* 2017; 4: 1400507.

5. Liu C, Li M and Fu W. Principles and apparatus of multi-point forming for sheet metal. *The International Journal of Advanced Manufacturing Technology* 2008; 35: 1227-1233.

6. Chen J, Fu W and Li M. Local bending effect and its controlling methods in multi-point forming. *The International Journal of Advanced Manufacturing Technology* 2017; 92: 4315-4322. journal article. DOI: 10.1007/s00170-017-0537-1.

7. Li M, Cai Z, Sui Z, et al. Principle and applications of multi-point matched-die forming for sheet metal. *Proceedings of the Institution of Mechanical Engineers, Part B: Journal of Engineering Manufacture* 2008; 222: 581-589.

8. Zhang H, Lu B, Chen J, et al. Thickness control in a new flexible hybrid incremental sheet forming process. *Proceedings of the Institution of Mechanical Engineers, Part B: Journal of Engineering Manufacture* 2017; 231: 779-791.

9. Abosaf M, Essa K, Alghawail A, et al. Optimisation of multi-point forming process parameters. *The International Journal of Advanced Manufacturing Technology* 2017; 92: 1849-1859. journal article. DOI: 10.1007/s00170-017-0155-y.

10. Mole N, Cafuta G and Štok B. A 3D forming tool optimisation method considering springback and thinning compensation. *Journal of Materials Processing Technology* 2014; 214: 1673-1685. DOI: https://doi.org/10.1016/j.jmatprotec.2014.03.017.

11. Davoodi B and Zareh-Desari B. Assessment of forming parameters influencing spring-back in multi-point forming process: a comprehensive experimental and numerical study. *Materials & Design* 2014; 59: 103-114.

12. Cai Z-Y, Wang S-H and Li M-Z. Numerical investigation of multi-point forming process for sheet metal: wrinkling, dimpling and springback. *The International Journal of Advanced Manufacturing Technology* 2008; 37: 927-936. journal article. DOI: 10.1007/s00170-007-1045-5.

13. Jia B-b and Wang W-W. New process of multi-point forming with individually controlled force-displacement and mechanism of inhibiting springback. *The International Journal of Advanced Manufacturing Technology* 2017; 90: 3801-3810. journal article. DOI: 10.1007/s00170-016-9709-7.

14. Tolipov AA, Elghawail A, Shushing S, et al. Experimental research and numerical optimisation of multi-point sheet metal forming implementation using a solid elastic cushion system. *Journal of Physics: Conference Series* 2017; 896: 012120. DOI: 10.1088/1742-6596/896/1/012120.

15. Kreuzer M. Strain measurement with fiber Bragg grating sensors. *HBM, Darmstadt, S2338-10 e* 2006.

16. Abushagur AAG, Arsad N, Reaz MI, et al. Advances in Bio-Tactile Sensors for Minimally Invasive Surgery Using the Fibre Bragg Grating Force Sensor Technique: A Survey. *Sensors-Basel* 2014; 14: 6633-6665. Review. DOI: 10.3390/s140406633.

17. Allwood G, Wild G and Hinckley S. Fiber Bragg Grating Sensors for Mainstream Industrial Processes. *Electronics* 2017; 6: 19. Review. DOI: 10.3390/electronics6040092.

18. Majumder M, Gangopadhyay TK, Chakraborty AK, et al. Fibre Bragg gratings in structural health monitoring - Present status and applications. *Sens Actuator A-Phys* 2008; 147: 150-164. Review. DOI: 10.1016/j.sna.2008.04.008.

19. Kersey AD, Davis MA, Patrick HJ, et al. Fiber grating sensors. *Journal of lightwave technology* 1997; 15: 1442-1463.

20. Panciroli R, Biscarini C, Giovannozzi A, et al. Structural Health Monitoring through Fiber Bragg Grating Strain Sensing. In: Simos TE and Tsitouras C (eds) *Proceedings of the International Conference of Numerical Analysis and Applied Mathematics 2014*. Melville: Amer Inst Physics, 2015.

21. Matveenko VP, Shardakov IN, Voronkov AA, et al. Measurement of strains by optical fiber Bragg grating sensors embedded into polymer composite material. *Struct Control Health Monit* 2018; 25: 11. Article. DOI: 10.1002/stc.2118.

22. Marsili R, Rossi G and Speranzini E. Fibre Bragg Gratings for the Monitoring of Wooden Structures. *Materials* 2018; 11: 18. Article. DOI: 10.3390/ma11010007.

23. Zeleny R and Vcelak J. Strain measuring 3D printed structure with embedded fibre Bragg grating. In: Barsony I, Zolnai Z and Battistig G (eds) *Proceedings of the 30th Anniversary Eurosensors Conference - Eurosensors 2016*. Amsterdam: Elsevier Science Bv, 2016, pp.1338-1341.

24. Wang Q, Huang J, Liu Q, et al. Dynamic strain measurement of hydraulic system pipeline using fibre Bragg grating sensors. *Adv Mech Eng* 2016; 8: 8. Article. DOI: 10.1177/1687814016645069.

25. Huang J, Zhou ZD, Zhang L, et al. Strain Modal Analysis of Small and Light Pipes Using Distributed Fibre Bragg Grating Sensors. *Sensors-Basel* 2016; 16: 11. Article. DOI: 10.3390/s16101583.

26. Weraneck K, Heilmeier F, Lindner M, et al. Strain Measurement in Aluminium Alloy during the Solidification Process Using Embedded Fibre Bragg Gratings. *Sensors-Basel* 2016; 16: 17. Article. DOI: 10.3390/s16111853.

27. Ramalingam RK, Klaser M, Schneider T, et al. Fiber Bragg Grating Sensors for Strain Measurement at Multiple Points in an NbTi Superconducting Sample Coil. *IEEE Sens J* 2014; 14: 873-881. Article. DOI: 10.1109/jsen.2013.2290153.

28. Mandal S, Pal A and Nagahanumaiah. Time-varying process model for intelligent prediction of strain and temperature in micro-turning process. *Proceedings of the Institution of Mechanical Engineers, Part B: Journal of Engineering Manufacture* 2017: 0954405417708223.

29. Lim SC, Lee HK and Park J. Grip force measurement of forceps with fibre Bragg grating sensors. *Electron Lett* 2014; 50: 733-735. Article. DOI: 10.1049/el.2013.4182.

30. Liang MF and Fang XQ. Application of Fiber Bragg Grating Sensing Technology for Bolt Force Status Monitoring in Roadways. *Appl Sci-Basel* 2018; 8: 12. Article. DOI: 10.3390/app8010107.

31. Su Y, Zhu Y, Zhang BF, et al. Real-time transverse force sensing using fiber Bragg grating through direct Stokes parameters measurement. *Opt Express* 2015; 23: 32300-32310. Article. DOI: 10.1364/oe.23.032300.

32. Kisala P and Cieszczyk S. Method of simultaneous measurement of two direction force and temperature using FBG sensor head. *Appl Optics* 2015; 54: 2677-2687. Article. DOI: 10.1364/ao.54.002677.

33. Kim C and Lee CH. Development of a 6-DoF FBG force-moment sensor for a haptic interface with minimally invasive robotic surgery. *J Mech Sci Technol* 2016; 30: 3705-3712. Article. DOI: 10.1007/s12206-016-0732-2.

34. Li XL. Monitoring the inner force of the frame-shear wall structure with MR dampers by FBG sensors. In: Zhou XJ (ed) *Advances in Structural Engineering, Pts 1-3*. Stafa-Zurich: Trans Tech Publications Ltd, 2011, pp.1031-1035.

35. Liu M, Zhang Z, Zhou Z, et al. A new method based on Fiber Bragg grating sensor for the milling force measurement. *Mechatronics* 2015; 31: 22-29.

36. Prasad AG, Anitha M, Rao KN, et al. Measurement of stress-strain response of a rammed earth prism in compression using fiber bragg grating sensors. *International Journal on Smart Sensing and Intelligent Systems* 2011; 4: 376-387.

37. Majumder M, Gangopadhyay TK, Chakraborty AK, et al. Fibre Bragg gratings in structural health monitoring—Present status and applications. *Sensors and Actuators A: Physical* 2008; 147: 150-164.

38. Li M, Liu Y, Su S, et al. Multi-point forming: a flexible manufacturing method for a 3-d surface sheet. *Journal of Materials Processing Technology* 1999; 87: 277-280.

39. Smart-Fibres-Ltd. SmartScan, https://www.smartfibres.com/products/smartscan (2018).

40. Abosaf M. *Finite Element Modelling of Multi-Point Forming*. University of Birmingham, Doctoral Dissertations, 2017.